Macromolecules

Article

Cite This: Macromolecules 2018, 51, 4049−4058

Stabilizing the Ordered Bicontinuous Double Diamond Structure of Diblock Copolymer by Configurational Regularity

Chih-Hsuan Lin,[†] Takeshi Higuchi,[‡] Hsin-Lung Chen,*[,†] Jing-Cherng Tsai,[§] Hiroshi Jinnai,*[,‡] and Takeji Hashimoto*[,∥]

[†]Department of Chemical Engineering and Frontier Research Center on Fundamental and Applied Sciences of Matters, National Tsing Hua University, Hsinchu 30013, Taiwan

[‡]Institute of Multidisciplinary Research for Advanced Materials (IMRAM), Tohoku University, 2-1-1, Katahira, Aoba-ku, Sendai, 980-8577, Japan

[§]Department of Chemical Engineering, National Chung Cheng University, Chia-Yi 62102, Taiwan

[∥]Kyoto University, Kyoto 606-6501, Japan

Supporting Information

ABSTRACT: We investigate the formation of the ordered bicontinuous structures in a stereoregular diblock copolymer, isotactic polypropylene-*block*-polystyrene (iPP-*b*-PS), in which the minority PP block possessed isotactic configuration. This diblock displayed the conventional ordered bicontinuous double gyroid (OBDG) morphology upon heating above the crystal melting point of the iPP block from the as-cast state. The OBDG phase remained stable in the heating process up to the order−disorder transition. In the subsequent cooling process from the nearly disordered state, the OBDG phase first developed, but when the temperature was sufficiently low, an order−order transition from OBDG to the ordered bicontinuous double diamond (OBDD) phase occurred, and OBDD eventually became the dominant structure. The results attested that OBDD and OBDG represented the thermodynamically stable structure at the lower and the higher temperature, respectively, and the OBDG morphology formed in the as-cast state was metastable. The present finding along with that of the syndiotactic polypropylene-*block*-polystyrene (sPP-*b*-PS) reported previously consolidated the role of configurational regularity in stabilizing the otherwise unstable OBDD phase for diblock copolymers. The stability of the OBDD structure was attributed to the cooperative effect of the relatively high polydispersity and the helical segment formation of the stereoregular minority block, as the conformational entropy loss arising from the packing frustration of the minority block in the network domain was effectively compensated by the release of enthalpy via the formation of helical segments and their associations.

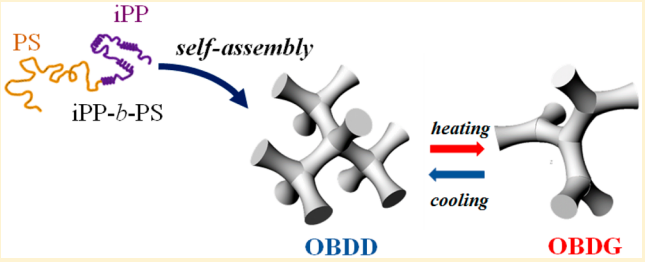

INTRODUCTION

Block copolymers exhibit a variety of long-range ordered nanostructures generated by the microphase separation between the constituent blocks. One-dimensionally stacked lamellae, hexagonally packed cylinders (HEX), and BCC-packed spheres represent the classical structures formed by diblock copolymers.[1] In between the lamellar and HEX phase, a narrow composition region called the "complex phase window" exists, in which the diblock copolymer may form spatially bicontinuous morphology.[2−5] The spatial continuity of the microdomain coupled with the high specific surface area offered by the bicontinuous structures expands the application window of diblock copolymers in the areas of catalysis,[6,7] photonics,[8−10] and optoelectronics.[11,12]

One fascinating feature of the bicontinuous morphology is that the network structures formed are long range ordered with well-defined space symmetries and numbers of pods radiating from a given node, n_p. In the case of diblock copolymers, three types of ordered bicontinuous structure have been identified, namely, ordered bicontinuous double gyroid (OBDG), ordered bicontinuous double diamond (OBDD), and *Fddd*. Both OBDG and OBDD are characterized by the cubic unit cells, with OBDG constructed by the tripods (n_p = 3) interconnected with $Ia\bar{3}d$ symmetry[13,14] and OBDD by the tetrapods (n_p = 4) interconnected with $Pn3m$ symmetry.[2,15] The single network *Fddd* structure with noncubic unit cell belongs to the O^{70} space group with a 3-fold symmetry (n_p = 3).[16]

OBDG is the predominantly observed bicontinuous structure of diblock copolymers. Indeed, it has long been believed that OBDD is always unstable relative to OBDG due to high packing frustration of the minority block chains around the nodes of the tetrapods, which causes the nonuniform stretching of the minority chains for attaining the incompressibility.[5,17] It is hence conceivable that once the packing frustration around

Received: November 12, 2017
Revised: May 4, 2018
Published: May 18, 2018

Downloaded via SYNCHROTRON RADIATION RESEARCH on January 21, 2019 at 03:46:40 (UTC).
See https://pubs.acs.org/sharingguidelines for options on how to legitimately share published articles.

© 2018 American Chemical Society

DOI: 10.1021/acs.macromol.7b02404
Macromolecules 2018, 51, 4049−4058

the nodes of the microdomain may be relieved, the stability of OBDD may supersede that of OBDG.[18,19] This postulate has been demonstrated to be true in a recent study by Takagi et al., which showed that OBDD structure formed in a dry-brush blend of a polystyrene-*block*-polyisoprene (PS-*b*-PI) and PI homopolymer (h-PI), wherein the solubilization of h-PI into the PI microdomain may release the packing frustration of PI block.[20,21] The OBDD structure of this blend was found to undergo an order−order transition (OOT) to OBDG upon heating.[20,21]

Recently, we discovered that OBDD existed as the thermodynamically equilibrium bicontinuous structure at the lower temperature in a neat diblock copolymer composed of a stereoregular block, syndiotactic polypropylene-*block*-polystyrene (sPP-*b*-PS), in which the minority PP block chains forming the tetrapod network domain possessed syndiotactic configuration.[22,23] The thermally induced OOT from OBDD to OBDG also occurred upon heating above the melting point of sPP in this system. The stability of the OBDD structure in sPP-*b*-PS was attributed to the ability of the sPP block to form helical segments even above its crystal melting point (T_m^{sPP}). At the lower temperature (but above T_m^{sPP}), the helical segments in higher population and their association to form a mesophase may effectively reduce the enthalpy inside the minority tetrapod domain, which was thought to compensate the conformational entropy loss of the minority block chains arising from the packing frustration around the nodes.[22,23]

The present work consolidates the role of configurational regularity in stabilizing the OBDD phase via studying the microphase-separated structure and the phase transition behavior of another stereoregular diblock copolymer, isotactic polypropylene-*block*-polystyrene (iPP-*b*-PS), wherein the minority PP block possesses *isotactic* configuration. We will demonstrate that the iPP-*b*-PS system also exhibited OBDD morphology and thermally induced OBDG-OBDD transition above the melting point of iPP; nevertheless, its phase transition pathway was different from that of sPP-*b*-PS. The observed phase transition behavior will be explained by considering the "anchoring effect" arising from the interhelix association of the stereoregular block chains on the activation barrier for the chain diffusion along the interface involved by the OOT. Moreover, we will address the significance of the release of enthalpy via the helical segment formation and its resultant interhelix association by the stereoregular block for stabilizing the OBDD structure with the consideration of its relatively large polydispersity.

EXPERIMENTAL SECTION

Materials and Sample Preparation. The iPP-*b*-PS diblock copolymer with the number-average molecular weights of iPP and PS blocks of 5500 and 11 500 g/mol, respectively, and the polydispersity index (PDI) of 1.19 was synthesized according to the procedure reported previously.[24] The purification of the synthesized iPP-*b*-PS was accomplished in two steps to remove the excess homopolymers. First, the excess PS (soluble in boiling acetone) was removed by Soxhlet extraction in boiling acetone. The resulting acetone-insoluble fraction was collected, dried, and allowed to undergo a second Soxhlet extraction with heptane to remove the residual tosyl group end-capped iPP. The resulting heptane-insoluble fraction was collected and dried under vacuum overnight to yield the pure iPP-*b*-PS as a white solid. The successful preparation of the structurally well-defined iPP-*b*-PS sample was demonstrated by the GPC curves shown in Figure S1 of the Supporting Information.

The volume fraction of iPP block in the copolymer was $f_{iPP} = 0.34$, as calculated from the molecular weights of iPP and PS block and the corresponding bulk densities 0.946 and 1.040 g/cm^3 at 298 K, respectively. For the film preparation, the diblock copolymer was dissolved in xylene at 50 °C, and the solution was subsequently cast on the Petri dish. A iPP-*b*-PS film was obtained after evaporating most of the solvent on a hot plate at ca. 140 °C followed by drying in vacuum at 70 °C for 24 h.

X-ray Scattering Measurement. The morphology of the iPP-*b*-PS was probed by small-angle X-ray scattering (SAXS) experiment performed at the Endstation BL23A1 of the National Synchrotron Radiation Research Center (NSRRC), Taiwan. The energy of X-ray source and the sample-to-detector distance was 15 keV and about 3000 mm, respectively. The scattering signals were collected by a Pilatus-1MF detector with 981 × 1043 pixel resolution. The wide-angle X-ray scattering (WAXS) data of the sample were collected simultaneously using a CMOS C9728DK flat panel detector. For the temperature-dependent study, the sample was equilibrated at each temperature for 5 min followed by data acquisition for 20 and 10 s for SAXS and WAXS measurement, respectively. The heating and cooling rates in the temperature-dependent experiments were both 5 °C/min with the accuracy of temperature control of ±0.5 °C. The scattering profiles were presented as the plot of the scattering intensity (I) versus the scattering wave vector, $q = 4\pi/\lambda \sin \theta/2$ (θ = scattering angle). The SAXS intensity was corrected for the incident beam intensity, the detector sensitivity, and the background arising from the air scattering.

Transmission Electron Microscopy (TEM) and Transmission Electron Microtomography (TEMT) Observations. The iPP-*b*-PS film was ultramicrotomed to a thickness of ca. 100 nm by using an ultramicrotome (UC7, Leica microsystems, Germany) with a diamond knife at −50 °C. The ultrathin section was transferred onto a Cu mesh with a polyvinylformal (PVF) supporting membrane. The thin section was stained with RuO_4 vapor (500 Pa) for 30 min. Prior to the electron microscopy experiments, gold naonparticles (diameter: 5 nm) were placed on the backside of supporting membrane. The thin section was observed by a TEM operated at 200 kV (JEM-2200FS, JEOL Ltd., Japan), and the system was equipped with a slow-scan CCD camera (Gatan USC 4000, Gatan Inc., USA). A series of TEM images were acquired at the tilt angles of ±73° in 1° step. The TEM images were aligned by the fiducial marker method[25] with Au nanoparticles deposited on a supporting membrane. After the alignment, the tilt series of the TEM images were reconstructed by a filtered back projection algorithm.[26] The 3D structure was visualized by manual segmentation and surface rendering using Amira software (Thermo Fisher Scientific, USA). Detailed experimental examples and related analytical methods can be found elsewhere.[27]

Fourier Transform Infrared Spectroscopy (FTIR) Measurement. The infrared absorption spectra of the iPP-*b*-PS at different temperatures were collected at a resolution of 4 cm^{-1} over 16 scans using a PerkinElmer Spectrum Two FTIR spectrophotometer. The sample was melt cast directly onto a KBr pellet to obtain a layer of thin film on KBr. The sample was equilibrated at each temperature for 5 min prior to data acquisition. The IR spectra of the sample at different temperatures were collected in a heating and cooling cycle.

RESULTS AND DISCUSSION

Observations of the OBDD Structure and the OBDG−OBDD Transition. SAXS has been widely utilized to identify the structures of diblock copolymers based upon the relative positions of the diffraction peaks. OBDG structure exhibits a series of diffraction peaks with the position ratio of $1:(4/3)^{1/2}:(7/3)^{1/2}:(8/3)^{1/2}:(10/3)^{1/2}:(11/3)^{1/2}$, corresponding to (211), (220), (321), (400), (420) and (332) diffraction plane, respectively;[20−23,28] the OBDD phase shows the diffraction peaks with the position ratio of $1:(3/2)^{1/2}:2^{1/2}:3^{1/2}:4^{1/2}$ which are associated with (110), (111), (200), (211), and (220) plane, respectively.[15,20−23,29] The obvious difference in the position of the second-order peak relative to that of the primary

DOI: 10.1021/acs.macromol.7b02404
Macromolecules 2018, 51, 4049−4058

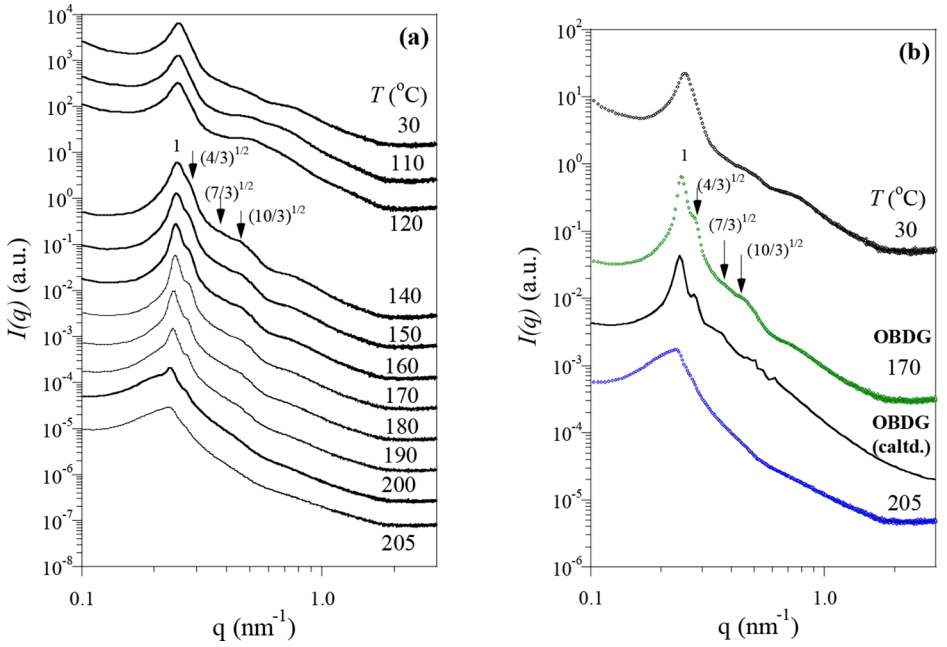

Figure 1. (a) Temperature-dependent SAXS profiles of the iPP-*b*-PS collected in a heating cycle from the as-cast state. (b) Enlarged SAXS profiles collected at 30, 170, and 205 °C for clearer identification of the scattering peaks; the SAXS curve calculated by the paracrystalline model of OBDG structure is also displayed for comparison.

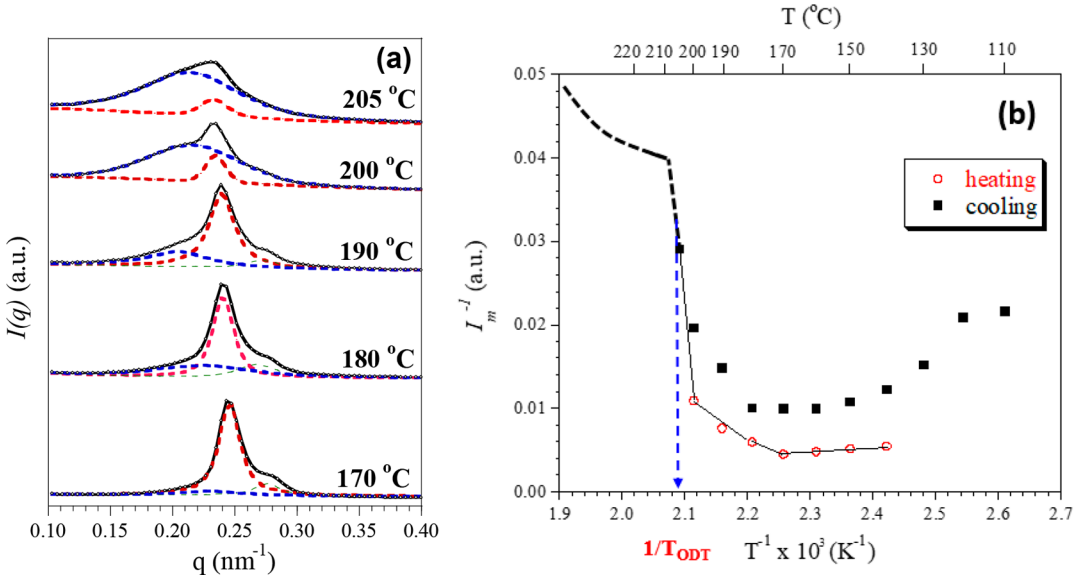

Figure 2. (a) SAXS profiles with the intensities presented in linear scale expanded in the q range of 0.1−0.4 nm^{-1} over the temperature range of 170−205 °C, where each observed profile shown by the solid line was decomposed into a broad peak with the peak at $q_{m1} \cong 0.21$ nm^{-1} (the blue broken line) and a sharp peak with the peak at $q_{m2} \cong 0.24$ nm^{-1} (the brown broken line) by the least-squares fit. (b) Plot of the inverse of the primary peak intensity against the inverse of the absolute temperature for the heating and cooling cycle using the SAXS data in Figures 1 and 3. For the heating cycle, the plot shows an abrupt rise of I_m^{-1} with T above 200 °C; in this case, the dashed line drawn for temperature above 205 °C is to project how the intensity could vary beyond this temperature according to the typical appearance of the I_m^{-1} vs T^{-1} plot in the ODT region.[34] According to this projection, T_{ODT} of the present system should locate near 205 °C.

peak can in particular be used to distinguish between these two structures by the SAXS profile.[22,23]

Figure 1a displays the temperature-dependent SAXS profiles of the iPP-*b*-PS collected in a heating cycle from the as-cast state. The SAXS curve at 30 °C showed a primary peak without clear higher-order peaks, indicating that the microphase-separated morphology was distorted by the crystallization of the iPP block occurred during solvent casting, as evidenced by its crystallinity of about 40% determined from the corresponding WAXS curve (see Figure S2). The higher-order peaks became discernible as the copolymer was heated above 140 °C, where the iPP crystallites were melted. Therefore, the present study focused on the self-assembly of the iPP-*b*-PS in the melt state to avoid the disturbance of crystallinity on the microphase-separated morphology. Between 150 and 200 °C, a set of scattering peaks with the position ratio of $1:(4/3)^{1/2}:(7/3)^{1/2}:(10/3)^{1/2}$ was identified, as demonstrated more clearly in the enlarged SAXS curve at 170 °C in Figure 1b, signaling

DOI: 10.1021/acs.macromol.7b02404
Macromolecules 2018, 51, 4049−4058

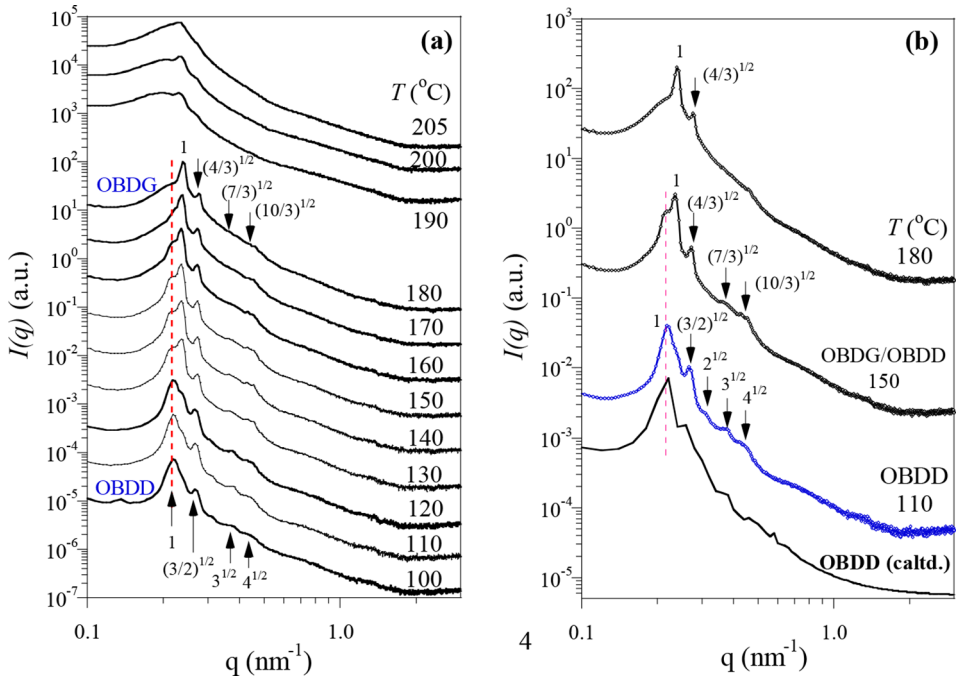

Figure 3. (a) Temperature-dependent SAXS profiles of the iPP-*b*-PS collected in a cooling cycle from 205 °C. (b) Enlarged SAXS profiles collected at 180, 150, and 110 °C for clearer identification of the scattering peaks; the SAXS curve calculated by the paracrystalline model of OBDD structure is also displayed for comparison.

that the copolymer formed the OBDG structure. The formation of the OBDG phase was further demonstrated by the close agreement between the observed SAXS profile and the scattering curve calculated by the paracrystalline model,[22] as shown in Figure 1b.

A detailed examination of the SAXS profiles at $T \geq 170$ °C revealed that the sharp diffraction peaks indeed overlapped with a broad component with the peak centering at ca. 0.21−0.23 nm^{-1}. This broad component may arise either from (i) the disordered phase or (ii) the anisotropic thermal composition fluctuations in the ordered phase. The scattering from the ordered phase having anisotropic composition fluctuations was theoretically developed by Shi, Noolandi, and Desai[30] and analyzed[31] for the lamellar, cylindrical, spherical, and hexagonally perforated lamellar phase, though such a scattering from the OBDG phase was not reported. Figure 2a presents the SAXS profiles at 170−205 °C expanded in the q range of 0.1−0.4 nm^{-1}, where each observed profile shown by the solid line was decomposed into a broad peak at the position q_{m1} (the blue broken line) and a sharp peak at the position q_{m2} nearly equal to 0.24 nm^{-1} by the least-squares fit. Both the broad and sharp peaks broadened with increasing temperature.

The sharp peak at q_{m2} was associated with the ordered OBDG phase, and the broad peak at q_{m1} may arise from (i) the disordered phase or (ii) the OBDG phase subjected to the anisotropic composition fluctuations. Considering these possible origins of the broad component, the scattering patterns observed at 170−205 °C may hence be interpreted by (scenario a) the thermal-fluctuation-driven order−disorder coexistence near the order-disorder transition (ODT) or (scenario b) the thermal composition fluctuations in a single OBDG phase. The first scenario has been investigated in detail for PS-*b*-PI by Koga et al.,[32,33] where the order−disorder coexistence was observed over a very narrow temperature window of ca. 4 K near the T_{ODT}. Since the broad and sharp peaks coexisted over a broad temperature range, the observed scattering behavior of the present iPP-*b*-PS at 170−205 °C was mainly attributed to the second scenario, i.e., the existence of anisotropic composition fluctuations in the OBDG phase, in particular in the lower temperature range of 170−200 °C.

Figure 2b displays the plot of the inverse of the primary peak intensity (I_m^{-1}) versus the inverse of absolute temperature (T^{-1}). The plot was seen to exhibit an abrupt rise of I_m^{-1} with T above ∼200 °C, which was reminiscent of the signature of the fluctuation-induced ODT.[34,35] Unfortunately, thermal degradation occurred above 205 °C, so that the I_m^{-1} vs T^{-1} plot could not be extended beyond this temperature for accurate determination of the ODT temperature (T_{ODT}). Nevertheless, considering that the abrupt rise of I_m^{-1} started above ∼200 °C and the fact that the broad component accounted for the major portion of the observed scattering profile at this temperature, the T_{ODT} should locate near 205 °C. Therefore, the SAXS profile at 205 °C was interpreted as that arising from the order−disorder coexistence near T_{ODT} (scenario a), and the diblock was considered to be in the nearly disordered state at this temperature.

Figure 3a shows the temperature-dependent SAXS profiles collected in the cooling process from 205 °C. A sharp peak at 0.238 nm^{-1} emerged as the diblock was cooled from 205 to 200 °C, signifying the development of an ordered phase. The diffraction peaks associated with the ordered structure became clearly discerned at 180 °C; in this case, the peak positions again followed the ratio of $1:(4/3)^{1/2}:(7/3)^{1/2}:(10/3)^{1/2}$, indicating the formation of OBDG structure from the disordered phase. Interestingly, an additional peak at 0.222 nm^{-1} developed beside the primary peak of the OBDG phase when the temperature was further lowered to 170 °C. This peak grew (the trend of which is shown by the change in the peak along broken line), while the OBDG primary peak diminished progressively with decreasing temperature. At 110

DOI: 10.1021/acs.macromol.7b02404
Macromolecules 2018, 51, 4049−4058

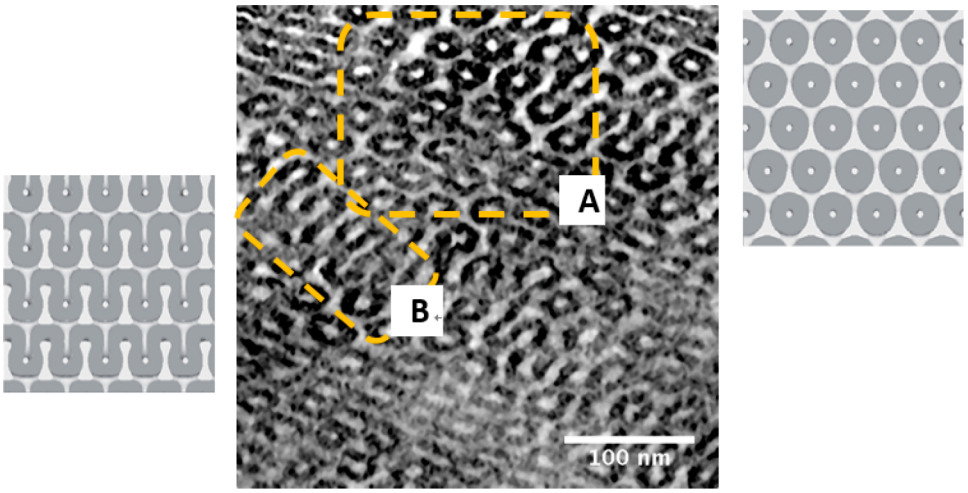

Figure 4. Reconstructed 2D TEM image of iPP-*b*-PS specimen stained with RuO_4. The bright and dark regions correspond to iPP and PS phase, respectively, due to the selective staining of PS block by RuO_4. The observed images in region A and region B can be simulated by the projections from the [111] and [211] directions of the OBDD lattice, respectively, as shown in the figure.

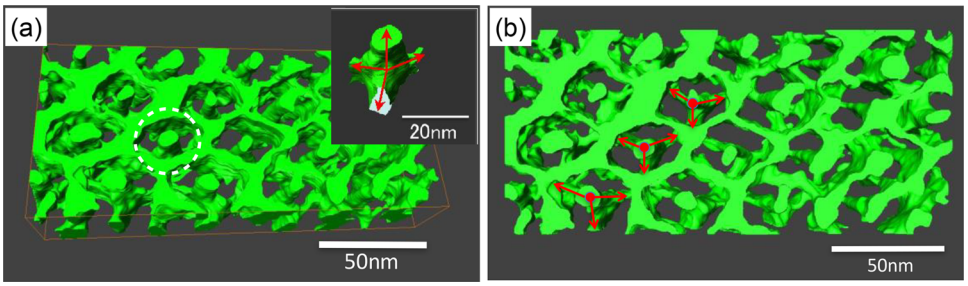

Figure 5. Three-dimensional TEM images of iPP phase from (a) oblique and (b) top views. The inset of (a) is the close-up image of connecting node with four branches.

and 100 °C, where the OBDG peak was nil, the positions of the diffraction peaks followed the ratio of $1:(3/2)^{1/2}:2^{1/2}:3^{1/2}:4^{1/2}$, as shown more clearly in Figure 3b, which was consistent with the relative peak positions prescribed by the OBDD structure. The formation of the OBDD phase was confirmed by the close agreement between the observed SAXS profile and the calculated scattering curve using the paracrystalline model of OBDD structure, as demonstrated in Figure 3b. The facts that the OBDG phase developed at the higher temperature and an OOT from OBDG to OBDD occurred upon cooling attested that OBDG and OBDD was the stable structure at the higher and the lower temperature, respectively.

The characteristic spacing of the (hkl) plane, d_{hkl}, of both OBDG and OBDD structures can be calculated by[2,29]

$$d_{hkl} = \frac{a_i}{\sqrt{h^2 + k^2 + l^2}} \quad (1)$$

where a_i is the lattice parameter of the cubic unit cell with i = D or G corresponding to OBDD and OBDG, respectively. The first-order scattering peak of OBDG and OBDD phase corresponds to (211) and (110) diffraction, respectively; the ratio of the characteristic spacing of these two diffraction planes has been derived based on the conservation of the microdomain volume across the OOT as $d_{110,D}/d_{211,G} = 1.09$.[23] The ratio calculated from the primary peak positions of the SAXS curves in Figure 3 was 1.08, which agreed very well with the theoretical value.

The formation of the OBDD structure in the iPP-*b*-PS was further verified by the real-space observation of the morphology by TEM using the sample cooled from 205 to 140 °C followed by annealing for 24 h to ensure that OBDD phase was well developed. Figure 4 displays the representative 2D TEM micrograph. The bright and dark region corresponded to iPP and PS phase, respectively, due to the selective staining of PS block by RuO_4. The observed image of the wagon-wheel lattice[15] in region A and the other image in region B can be simulated by the projections from the [111] and [211] directions of the OBDD lattice, respectively,[23] as shown in Figure 4.

To consolidate the real-space picture of the OBDD structure, TEMT was further conducted here to reveal the 3D structure. Figure 5 shows the representative 3D images of the iPP phase in the iPP-*b*-PS specimen. The volume fraction of iPP phase evaluated from the 3D image was 0.32, which closely agreed with that (f_{iPP} = 0.34) calculated from the block molecular weights. As indicated by the red arrows in the inset of Figure 5a and those in Figure 5b, the iPP blocks formed tetrapod microdomains interconnected into a network, which was consistent with the OBDD morphology. It is noted that the sample for TEM observation was cooled to room temperature followed by microtoming at −50 °C after annealing at 140 °C; in this case, the crystallization of iPP block invariably took place at the lower temperatures, such that the OBDD morphology observed in the reconstructed 3D image was distorted. Nevertheless, the TEMT result showed unambiguously that tetrapod domains existed in the sample, which further

DOI: 10.1021/acs.macromol.7b02404
Macromolecules 2018, 51, 4049−4058

supported the formation of the OBDD structure in the iPP-*b*-PS studied.

Hysteresis of the OBDG−OBDD Transition. The temperature-dependent SAXS results revealed that similar to sPP-*b*-PS, the stereoregular diblock copolymer iPP-*b*-PS was able to form the OBDD structure and an OOT from OBDG to OBDD occurred in the cooling process. Nevertheless, there was difference in the phase transition behavior between the present iPP-*b*-PS and the previously studied sPP-*b*-PS.[22,23] In the sPP-*b*-PS system, the copolymer showed OBDD morphology in the as-cast state; the OBDD structure started to transform to OBDG upon heating to T_{OOT}, but ODT was not accessible upon further increasing temperature before chemical degradation due to its higher molecular weight, which prescribed a larger segregation strength.[22,23] Upon cooling the sPP-*b*-PS from the OBDG phase formed at the higher temperature, the OBDG structure transformed into OBDD, showing the thermal reversibility of the OOT. On the other hand, the iPP-*b*-PS displayed OBDG morphology in the as-cast state, which was distorted by the crystallization of iPP block. Since OBDD was the equilibrium structure at the lower temperature, such an OBDG morphology should be metastable in nature, as it was trapped into the bulk state during the solvent evaporation. This nonequilibrium OBDG phase is denoted as "t-OBDG".

Upon heating above the melting point of iPP ($T > T_m^{iPP} \approx 140$ °C), the t-OBDG phase did not transform into OBDD in the temperature range ($T < 170$ °C) where OBDD was supposed to be the stable structure, implying that the activation barrier of the t-OBDG-to-OBDD transition in the heating process was high. We annealed the as-cast sample at 150 °C for 24 h to examine if the prolonged annealing was able to induce the transformation of t-OBDG to OBDD phase. The SAXS profile of this annealed sample is displayed in Figure S3. It was found that the scattering peaks still displayed the position ratios prescribed by the OBDG structure, indicating that t-OBDG did not transform into OBDD phase even upon the prolonged annealing, which was consistent with the suggestion of the high activation barrier.

When the sample was heated to the disordered state to erase the solvent-cast history, the equilibrium OBDG structure developed in the subsequent cooling from the nearly disordered phase was able to transform to OBDD starting at $T < 170$ °C. Why was the activation barrier of the t-OBDG-to-OBDD transition in the heating process from the as-cast state higher than the activation barrier from the equilibrium OBDG to OBDD in the cooling process? We propose that the helical segments formed by the iPP block might play an important role on such a hysteresis effect as described above due to the following reason. It is known that the helical conformation of the stereoregular polymers such as iPP and sPP in the crystalline state may persist above their melting points due to strong intramolecular coupling.[36−38] In this case, the helical segments with various lengths existed in the melt state with their population decreasing with increasing temperature.[36] The interaction between the helical segments could further lead to the formation of mesomorphic associations within the iPP microdomains. The OOT between OBDD and OBDG involving the translational diffusion of the chemical junctions of the block chains along the interface and the conformational reorganization of the iPP block chains may perturb the association state and the spatial distribution of the helical segments, which resulted in an activation barrier of the transition. Moreover, the association of the helices into the mesophase could impose an anchoring effect that suppressed the translational diffusion of the chemical junctions of the block chains along the interface which is crucial for the block copolymer to undergo OOT, as schematically illustrated in Figure 6. The anchoring effect was brought by the cooperative

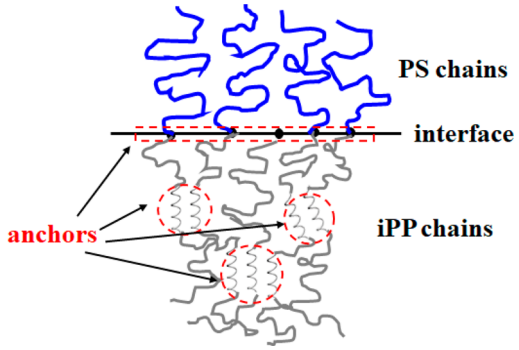

Figure 6. schematic illustrations of the interhelix associations which serve as "anchors" for the translational diffusion of the chemical junctions along the interface and thereby of block chains in the domain space.

confinements of (a) the chemical junctions on the interface and (b) the helix parts of the iPP block chains forming the interhelix associations which act as the physical cross-links for iPP block chains. This anchoring effect may slow down the chain dynamics dramatically and hence slow down or even hinder the OOT, depending on the population of the helical segments and resultant extent of the interhelix associations. It is worth noting that the anchoring effect was also proposed to raise T_{ODT} of the block copolymers which selectively incorporated the palladium nano-particles in one of the microdomains.[39]

Upon heating from the as-cast state, the OOT from t-OBDG to OBDD was supposed to take place right above the melting point, which was 140 °C in our heating protocol; in the minority domains of t-OBDG, the iPP helical segments may still be abundant, and the interhelix association may still be extensive. This may enlarge the activation barrier and retard the translational diffusion of the chemical junctions and block chains by the anchoring effect, which thereby slowed down the OOT process and hence hindered t-OBDG to transform into OBDD up to the ODT temperature under the present heating protocol. In the cooling process, OBDD became the stable structure below 170 °C, which was 30 °C higher than the expected onset of transition in the heating cycle; the lower helical segment population and the weaker or perturbed mesomorphic associations of the helices at the higher temperatures may bring about a lower activation barrier and faster translational diffusion of the block chains along the interface and hence allowed the OBDG-to-OBDD transition to take place under the present cooling protocol. Nevertheless, the transition from OBDG to OBDD on cooling process may still suffer from the anchoring effect, which led to the coexistence of OBDG and OBDD phases over the wide temperature range. Therefore, the anchoring effect caused by the interhelix association may dramatically slow down the dynamics of OOT from OBDD to OBDG (heating) as well as OBDG to OBDD (cooling, especially at low temperatures), thereby bringing about the large hysteresis. This anchoring effect is anticipated to be stronger in iPP-*b*-PS than in sPP-*b*-PS,

DOI: 10.1021/acs.macromol.7b02404
Macromolecules 2018, 51, 4049−4058

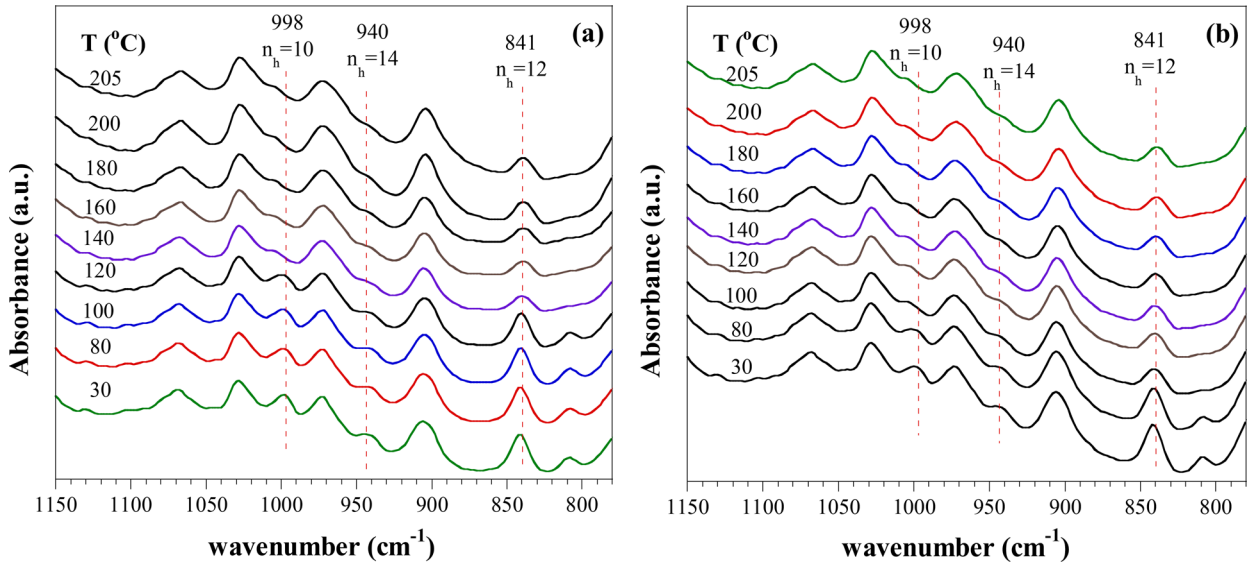

Figure 7. FTIR spectra in the region of 780−1150 cm^{-1} of the iPP-*b*-PS collected in (a) heating cycle and (b) cooling cycle. The minimum numbers of monomers (n_h) in the helical sequences of iPP for the appearance of the bands at 841, 940, and 998 cm^{-1} are 12, 14 and 10, respectively, as marked in the figures.

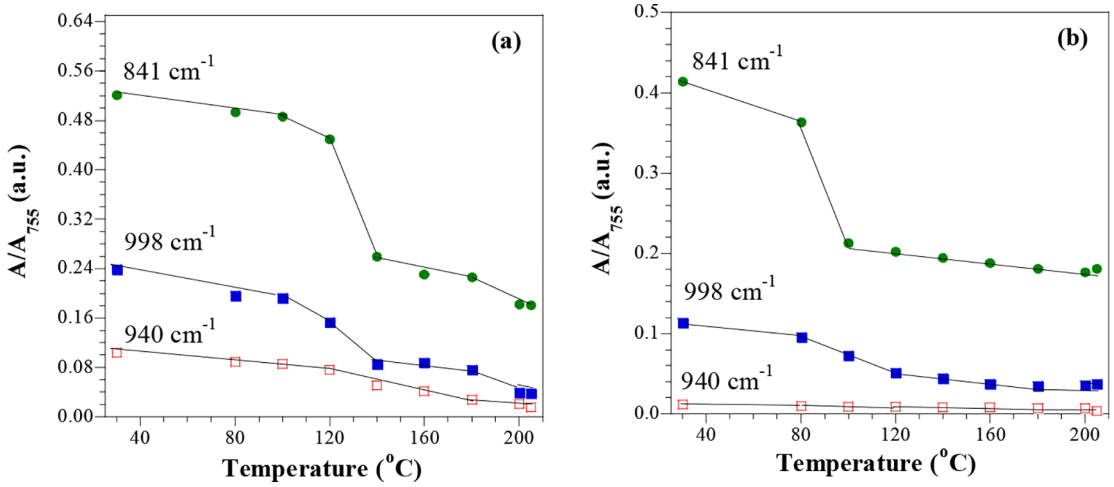

Figure 8. Temperature variations of the absorbancies of the three IR bands at 841, 940, and 998 cm^{-1} of iPP block relative to that of the PS peak at 755 cm^{-1} in (a) heating and (b) cooling cycle. The absorbancies were found to increase with decreasing temperature, showing a greater population of the helical segments at lower temperature. The abrupt changes of the absorbances were caused by the crystal melting and crystallization of iPP block in the heating and cooling cycle, respectively.

resulting in the larger hysteresis effect in iPP-*b*-PS than in sPP-*b*-PS.

The temperature dependence of the helical segment population of iPP block in the iPP-*b*-PS was evaluated by the FTIR spectra, as shown in Figure 7. For iPP, the various helical IR absorption bands arranged in terms of the degree of order from high to low are 940, 1220, 1167, 1303, 1330, 841, 998, 900, 808, 1100, and 973 cm^{-1}.[37,38] We focused on the three absorption peaks located at 841, 940, and 998 cm^{-1}, where the minimum numbers of monomers (n_h) in the helical sequences for the appearance of these bands are 12, 14, and 10, respectively. It can be seen that these bands were weaker at higher temperature, but they did not vanish completely even at 205 °C, confirming that the helical segments still persisted in the melt state. The temperature dependences of the peak intensities are manifested more clearly in Figure 8, which plots the absorbances of the three bands relative to the absorbance of the PS peak at 755 cm^{-1} as a function of temperature. For both heating and cooling cycles, the absorbances were found to increase with decreasing temperature, showing a greater population of the helical segments at lower temperatures. The absorbancies experienced an abrupt drop at 140 °C in the heating process due to the crystal melting, while the abrupt rise of the absorbancies near 100 °C in the cooling cycle arose from the occurrence of crystallization of iPP block. It is noted that in the melt state ($T \geq 140$ °C) the absorbancies of the three helix peaks at a given temperature observed in the heating cycle were consistently larger than those found in the cooling cycle (see Figure 8). This phenomenon was in accord with the thermo-irreversibility of the OOT process, as the higher population of the helical segments in the heating process from the as-cast state prescribed a higher activation barrier and slower chain diffusion for the OOT.

DOI: 10.1021/acs.macromol.7b02404
Macromolecules 2018, 51, 4049−4058

Thermodynamic Reasoning for the Enhancement of the Stability of OBDD Phase by Configurational Regularity. Our SAXS and TEM results have revealed the existence of OBDD structure and OBDG−OBDD OOT in an iPP-*b*-PS. Similar to the previously studied sPP-*b*-PS system, OBDD and OBDG represented the stable bicontinuous structure at the lower and the higher temperature, respectively. For diblock copolymers, OBDD has long been considered to be unstable relative to OBDG irrespective of the segregation strength. The dominance of OBDG has been ascribed to the weaker packing frustration of the minority blocks forming the network microdomains, as the self-consistent field calculation revealed a smaller deviation of the mean curvature of an OBDG tripod from constant mean curvature than that associated with a tetrapod in OBDD.[17] The thermodynamic stability of OBDG relative to OBDD has also been verified from the calculated local surface area-to-volume ratio by Hyde et al.[40] Consequently, relieving the conformational entropy penalty associated with the packing frustration of the minority block chains is a key for stabilizing OBDD phase. This has been demonstrated by blending the diblock copolymer with the corresponding homopolymer, where the homopolymer chains were be localized to the node region to release the packing frustration of the minority block chains.[20,21]

In the case of neat stereoregular diblock copolymer, OBDD was found to emerge as the stable structure at the lower temperature. It should be noted that the polydispersity (PDI) of the iPP block in the present iPP-*b*-PS and sPP block in the previously studied sPP-*b*-PS were quite high (cf. PDI of iPP block = 1.39; see Figure S1). It may hence be speculated that the relatively broad distribution of iPP chain length may effectively alleviate the packing frustration in the network domains, so as to enhance the stability of OBDD phase. The effect of polydispersity on the phase behavior of block copolymer has been well studied both theoretically and experimentally.[41] In the previous studies of poly(ethylene-*alt*-propylene)-*block*-poly(DL-lactide) (PEP-*b*-PLA), increasing the PDI of the minority PLA block was found to induce the transformation of lamellar phase to OBDG and eventually to cylinder structure (instead of OBDD), when the PDI of the PLA block was increased to as high as 1.85 (which was much higher than the value of 1.39 of the iPP block in the present iPP-*b*-PS system and 1.32 of the sPP block in the previous sPP-*b*-PS system).[42,43] Although the PDI can generally have a large impact on the microphase-separated morphology of diblock copolymers, it has never been observed or predicted that increasing the PDI of the minority block can stabilize OBDD structure relative to OBDG and bring about the thermally induced OOT between OBDG and OBDD. Consequently, we assert that the PDI effect alone is unable to stabilize OBDD phase, although this effect is anticipated to alleviate the packing frustration in the microdomains. Moreover, the PDI alone may also not be able to account for the large hysteresis effects observed in this work.

We postulate that the configurational regularity of the minority stereoregular block (i.e., iPP or sPP) plays an even more important role than the PDI effect in enhancing the stability of OBDD structure, as they can form helical segments. The free energy of the minority domain composes of both entropic and enthalpic contributions; the formation of the helical segments and the lateral packing of these segments to form mesomorphic associations may effectively lower the enthalpy of the minority domains. Consequently, the cost of the conformational entropy loss arising from the packing frustration, which is somewhat alleviated by the PDI effect, of the stereoregular minority blocks may be further compensated by the release of enthalpy in the minority domain via the formation of helical segments and resultant interhelix association, so that OBDD becomes the stable structure at sufficiently low temperatures where the helix population is high. It should be crucial to note also that the chain stretching to alleviate the packing frustrations further enhances the chain-stretching induced interhelix associations. Increasing temperature reduces the population of the helical segments and the interhelix associations. When the temperature is sufficiently high, the cost of the entropic loss arising from the packing frustration of the minority block becomes dominant over the enthalpic contribution, which then favors the OBDG structure.

CONCLUSIONS

The present study consolidates the concept of exploiting configurational regularity to stabilize the otherwise unstable OBDD morphology for diblock copolymers by showing that an iPP-*b*-PS displayed the thermodynamically stable OBDD structure and the thermally induced OBDG−OBDD transition. The iPP-*b*-PS was analogous to the previously studied sPP-*b*-PS system in terms of the thermodynamic stability of the bicontinuous morphology, where OBDD and OBDG corresponded to the thermodynamically stable structure at the lower and the higher temperature, respectively. However, the OBDG−OBDD OOT of the iPP-*b*-PS exhibited a strong hysteresis effect in the heating and subsequent cooling process, which was attributed to the anchoring effect arising from the interhelix association of the iPP blocks on the translational diffusions of the chemical junctions along the interface and the iPP block chains in the microdomain space. Depending on the population of the helical segments and the extent of the resultant interhelix associations, the anchoring effect may slow down the chain dynamics dramatically and hence even hinder the OOT. As a result, the metastable OBDG structure formed in the as-cast blend was unable to transform into OBDD on heating due to the stronger anchoring effect at the lower temperatures. In the cooling process, the lower helical segment population at the higher temperatures allowed the occurrence of OBDG-to-OBDD transition, although the transition still suffered from the anchoring effect. Finally, considering that the lower entropic penalty associated with the packing frustration of the minority block forming the network domain is the key factor that favors OBDG over OBDD, the thermodynamic stability of OBDD phase of the iPP-*b*-PS was ascribed to the configurational regularity of the stereoregular iPP block, in that the formation of the helical segments and the association of them into the mesophase reduced the enthalpy of the minority domain and, along with the polydispersity effect, released the free energy cost associated with the packing frustration of the minority block.

ASSOCIATED CONTENT

Supporting Information

The Supporting Information is available free of charge on the ACS Publications website at DOI: 10.1021/acs.macromol.7b02404.

GPC curves of iPP-*b*-PS and the corresponding homopolymers; temperature-dependent WAXS profiles collected simultaneously with the SAXS data in the

DOI: 10.1021/acs.macromol.7b02404
Macromolecules 2018, 51, 4049−4058

heating and subsequent cooling cycle and the corresponding temperature-dependent crystallinity; SAXS profile of iPP-*b*-PS having been treated by annealing the as-cast film at 150 °C for 24 h (PDF)

AUTHOR INFORMATION

Corresponding Authors

*(H.-L.C.) E-mail hlchen@che.nthu.edu.tw.
*(H.J.) E-mail hiroshi.jinnnai.d4@tohoku.ac.jp.
*(T.H.) E-mail hashi2@pearl.ocn.ne.jp.

ORCID

Hsin-Lung Chen: 0000-0002-3572-723X
Hiroshi Jinnai: 0000-0003-3400-1928

Notes

The authors declare no competing financial interest.

ACKNOWLEDGMENTS

This work is supported by the Ministry of Science and Technology (MOST) Taiwan under Grant MOST102-2221-E-007-136-MY3 and by JSPS KAKENHI Grants 16H06040, 16H02288, and 16K14001 Japan and also by the Management Expenses Grants for National Universities Corporations from Ministry of Education, Culture, Sports, Science and Technology of Japan (MEXT). We thank Ms. Akemi Kumagai for her assistance in TEM experiments.

REFERENCES

(1) Leibler, L. Theory of microphase separation in block copolymers. *Macromolecules* **1980**, *13* (6), 1602−1617.
(2) Hajduk, D. A.; Harper, P. E.; Gruner, S. M.; Honeker, C. C.; Kim, G.; Thomas, E. L.; Fetters, L. J. The gyroid: a new equilibrium morphology in weakly segregated diblock copolymers. *Macromolecules* **1994**, *27* (15), 4063−4075.
(3) Meuler, A. J.; Hillmyer, M. A.; Bates, F. S. Ordered network mesostructures in block polymer materials. *Macromolecules* **2009**, *42* (19), 7221−7250.
(4) Matsen, M. W.; Schick, M. Self-assembly of block copolymers. *Curr. Opin. Colloid Interface Sci.* **1996**, *1* (3), 329−336.
(5) Matsen, M. W.; Schick, M. Stable and unstable phases of a diblock copolymer melt. *Phys. Rev. Lett.* **1994**, *72* (16), 2660−2663.
(6) Hashimoto, T.; Tsutsumi, K.; Funaki, Y. Nanoprocessing based on bicontinuous microdomains of block copolymers: nanochannels coated with metals. *Langmuir* **1997**, *13* (26), 6869−6872.
(7) Adachi, M.; Okumura, A.; Sivaniah, E.; Hashimoto, T. Incorporation of metal nanoparticles into a double gyroid network texture. *Macromolecules* **2006**, *39* (21), 7352−7357.
(8) Martin-Moreno, L.; Garcia-Vidal, F.; Somoza, A. Self-assembled triply periodic minimal surfaces as molds for photonic band gap materials. *Phys. Rev. Lett.* **1999**, *83* (1), 73−75.
(9) Peng, S.; Zhang, R.; Chen, V. H.; Khabiboulline, E. T.; Braun, P.; Atwater, H. A. Three-dimensional single gyroid photonic crystals with a mid-infrared bandgap. *ACS Photonics* **2016**, *3* (6), 1131−1137.
(10) Urbas, A. M.; Maldovan, M.; DeRege, P.; Thomas, E. L. Bicontinuous cubic block copolymer photonic crystals. *Adv. Mater.* **2002**, *14* (24), 1850−1853.
(11) Crossland, E. J. W.; Kamperman, M.; Nedelcu, M.; Ducati, C.; Wiesner, U.; Smilgies, D. M.; Toombes, G. E. S.; Hillmyer, M. A.; Ludwigs, S.; Steiner, U.; Snaith, H. J. A bicontinuous double gyroid hybrid solar cell. *Nano Lett.* **2009**, *9* (8), 2807−2812.
(12) Liu, Z.; Li, Y.; Zhao, Z.; Cui, Y.; Hara, K.; Miyauchi, M. Block copolymer templated nanoporous TiO_2 for quantum-dot-sensitized solar cells. *J. Mater. Chem.* **2010**, *20* (3), 492−497.
(13) Jinnai, H.; Kajihara, T.; Watashiba, H.; Nishikawa, Y.; Spontak, R. J. Interfacial and topological measurements of bicontinuous polymer morphologies. *Physical Review E* **2001**, *64* (1), 010803.
(14) Jinnai, H.; Nishikawa, Y.; Spontak, R. J.; Smith, S. D.; Agard, D. A.; Hashimoto, T. Direct measurement of interfacial curvature distributions in a bicontinuous block copolymer morphology. *Phys. Rev. Lett.* **2000**, *84* (3), 518.
(15) Thomas, E. L.; Alward, D. B.; Kinning, D. J.; Martin, D. C.; Handlin, D. L., Jr.; Fetters, L. J. Ordered bicontinuous double-diamond structure of star block copolymers: a new equilibrium microdomain morphology. *Macromolecules* **1986**, *19* (8), 2197−2202.
(16) Takenaka, M.; Wakada, T.; Akasaka, S.; Nishitsuji, S.; Saijo, K.; Shimizu, H.; Kim, M. I.; Hasegawa, H. Orthorhombic Fddd network in diblock copolymer melts. *Macromolecules* **2007**, *40* (13), 4399−4402.
(17) Matsen, M. W.; Bates, F. S. Origins of complex self-assembly in block copolymers. *Macromolecules* **1996**, *29* (23), 7641−7644.
(18) Matsen, M. W. Phase behavior of block copolymer/homopolymer blends. *Macromolecules* **1995**, *28* (17), 5765−5773.
(19) Martínez-Veracoechea, F. J.; Escobedo, F. A. Monte Carlo study of the stabilization of complex bicontinuous phases in diblock copolymer systems. *Macromolecules* **2007**, *40* (20), 7354−7365.
(20) Takagi, H.; Yamamoto, K.; Okamoto, S. Ordered-bicontinuous-double-diamond structure in block copolymer/homopolymer blends. *EPL (Europhysics Letters)* **2015**, *110* (4), 48003.
(21) Takagi, H.; Takasaki, T.; Yamamoto, K. Phase Diagram for Block Copolymer and Homopolymer Blends: The Phase Boundary of the Ordered Bicontinuous Double Diamond Network Structure. *J. Nanosci. Nanotechnol.* **2017**, *17* (12), 9009−9014.
(22) Chu, C. Y.; Lin, W. F.; Tsai, J. C.; Lai, C. S.; Lo, S. C.; Chen, H. L.; Hashimoto, T. Order−Order Transition between Equilibrium Ordered Bicontinuous Nanostructures of Double Diamond and Double Gyroid in Stereoregular Block Copolymer. *Macromolecules* **2012**, *45* (5), 2471−2477.
(23) Chu, C. Y.; Jiang, X.; Jinnai, H.; Pei, R. Y.; Lin, W. F.; Tsai, J. C.; Chen, H. L. Real-space evidence of the equilibrium ordered bicontinuous double diamond structure of a diblock copolymer. *Soft Matter* **2015**, *11* (10), 1871−1876.
(24) Lin, M. C.; Chen, H. L.; Lin, W. F.; Huang, P. S.; Tsai, J. C. Crystallization of isotactic polypropylene under the spatial confinement templated by block copolymer microdomains. *J. Phys. Chem. B* **2012**, *116* (40), 12357−12371.
(25) Luther, P. K.; Lawrence, M. C.; Crowther, R. A. A method for monitoring the collapse of plastic sections as a function of electron dose. *Ultramicroscopy* **1988**, *24* (1), 7−18.
(26) Crowther, R. A.; DeRosier, D. J.; A. Klug, F. R. S. In *The Reconstruction of a Three-Dimensional Structure from Projections and Its Application to Electron Microscopy*, Proceedings of the Royal Society of London A: Mathematical, Physical and Engineering Sciences; The Royal Society: 1970; *317* (1530), pp 319−340.
(27) Jinnai, H.; Spontak, R. J.; Nishi, T. Transmission electron microtomography and polymer nanostructures. *Macromolecules* **2010**, *43* (4), 1675−1688.
(28) Vigild, M. E.; Almdal, K.; Mortensen, K.; Hamley, I. W.; Fairclough, J. P. A.; Ryan, A. J. Transformations to and from the Gyroid Phase in a Diblock Copolymer. *Macromolecules* **1998**, *31* (17), 5702−5716.
(29) Winey, K. I.; Thomas, E. L.; Fetters, L. J. The ordered bicontinuous double-diamond morphology in diblock copolymer/homopolymer blends. *Macromolecules* **1992**, *25* (1), 422−428.
(30) Shi, A.-C.; Noolandi, J.; Desai, R. C. Theory of anisotropic fluctuations in ordered block copolymer phases. *Macromolecules* **1996**, *29* (20), 6487−6504.
(31) Laradji, M.; Shi, A.-C.; Noolandi, J.; Desai, R. C. Stability of ordered phases in diblock copolymer melts. *Macromolecules* **1997**, *30* (11), 3242−3255.
(32) Koga, T.; Koga, T.; Hashimoto, T. Ultra-small-angle x-ray scattering studies on order-disorder transition in diblock copolymers. *J. Chem. Phys.* **1999**, *110*, 11076−11086.
(33) Koga, T.; Koga, T.; Kimishima, K.; Hashimoto, T. Long-range density fluctuations in a symmetric diblock copolymer. *Phys. Rev. E* **1999**, *60*, R3501−4.

DOI: 10.1021/acs.macromol.7b02404
Macromolecules 2018, 51, 4049−4058

(34) Sakamoto, N.; Hashimoto, T. Order-disorder transition of low molecular weight polystyrene-*block*-polyisoprene. 1. SAXS analysis of two characteristic temperatures. *Macromolecules* **1995**, *28* (20), 6825−6834.
(35) Bates, F. S.; Fredrickson, G. H. Block copolymer thermodynamics: theory and experiment. *Annu. Rev. Phys. Chem.* **1990**, *41*, 525−557.
(36) Zhu, X.; Fang, Y.; Yan, D. A possible explanation to the structure change of isotactic polypropylene occurring at about 135° C. *Polymer* **2001**, *42* (21), 8595−8598.
(37) Zhu, X.; Yan, D.; Yao, H.; Zhu, P. In situ FTIR spectroscopic study of the regularity bands and partial-order melts of isotactic poly (propylene). *Macromol. Rapid Commun.* **2000**, *21* (7), 354−357.
(38) Zhu, X.; Yan, D.; Fang, Y. In situ FTIR spectroscopic study of the conformational change of isotactic polypropylene during the crystallization process. *J. Phys. Chem. B* **2001**, *105* (50), 12461−12463.
(39) Zhao, Y.; Saijo, K.; Hashimoto, T. Order-disorder transition of nanocomposite: polystyrene-block-poly(methyl methacrylate) with palladium nanoparticles. *Macromolecules* **2013**, *46*, 957−970.
(40) Schröder-Turk, G. E.; Fogden, A.; Hyde, S. T. Local v/a variations as a measure of structural packing frustration in bicontinuous mesophases, and geometric arguments for an alternating Im $\bar{3}$ m phase in block-copolymers with polydispersity. *Eur. Phys. J. B* **2007**, *59* (1), 115−126.
(41) Lynd, N. A.; Meuler, A. J.; Hillmyer, M. A. Polydispersity and block copolymer self-assembly. *Prog. Polym. Sci.* **2008**, *33* (9), 875−893.
(42) Lynd, N. A.; Hillmyer, M. A. Influence of Polydispersity on the Self-Assembly of Diblock Copolymers. *Macromolecules* **2005**, *38* (21), 8803−8810.
(43) Lynd, N. A.; Hillmyer, M. A. Effects of polydispersity on the order-disorder transition in block copolymer melts. *Macromolecules* **2007**, *40* (22), 8050−8055.

DOI: 10.1021/acs.macromol.7b02404
Macromolecules 2018, 51, 4049−4058